Weiliang, Kong., Zhaochong, Zhang., Dongyang, Zhang., Changhong, Wang., M., Santosh., Bingxiang, Liu., and Bowen, Wei., 2022, New insights into deep carbon recycling and formation of nepheline-bearing alkaline rocks from Sr-Nd-Mg isotope compositions: GSA Bulletin, https://doi.org/10.1130/B36555.1.

Supplemental Material

Figure S1. Field photographs and photomicrographs of the nepheline syenite (plane-polarized light).

Figure S2. Harker diagram of major elements from clinopyroxene in nepheline syenite and nephelinite.

Figure S3. Primitive mantle-normalized trace element patterns and chondrite-normalized rare earth element patterns of the clinopyroxenes in Wajilitag nepheline syenite and nephelinite.

Figure S4. LOI versus Na_2O, Ba, Sr and Zr diagrams.

Figure S5. Rayleigh fractionation model showing the $\delta^{26}Mg$ evolution as fractional crystallization of ilmenite and spinel.

Table S1. Major element analyses of the clinopyroxene in the Wajilitag nepheline syenite, Tarim LIP, NW China.

Table S2. Trace element analyses of the clinopyroxene in the Wajilitag nepheline syenite and nephelinite, Tarim LIP, NW China.

Table S3. Sr isotopic compositions of the clinopyroxene in the Wajilitag nepheline syenite and nephelinite, Tarim LIP, NW China.

Table S4. Major element analyses of the alkali feldspar in the Wajilitag nepheline syenite, TLIP, Tarim LIP, NW China.

Table S5. Major element analyses of the nepheline in the Wajilitag nepheline syenite, Tarim LIP, NW China.

Table S6. Major element analyses of the sodalite in the Wajilitag nepheline syenite, Tarim LIP, NW China.

Table S7. Major element analyses of the titanite in the Wajilitag nepheline syenite, Tarim LIP, NW China.

Table S8. Major element analyses of the apatite in the Wajilitag nepheline syenite, Tarim LIP, NW China.

Table S9. Major (wt%) and trace (ppm) elements of the Wajilitag nepheline syenite, Tarim LIP, NW China.

Table S10. Zircon U–Pb ages of the Wajilitag nepheline syenite, Tarim LIP, NW China.

Table S11. Sr-Nd isotopic compositions of the Wajilitag nepheline syenite, Tarim LIP, NW China.

Table S12. Mg isotopic compositions of the Wajilitag nepheline syenite, Tarim LIP, NW China.

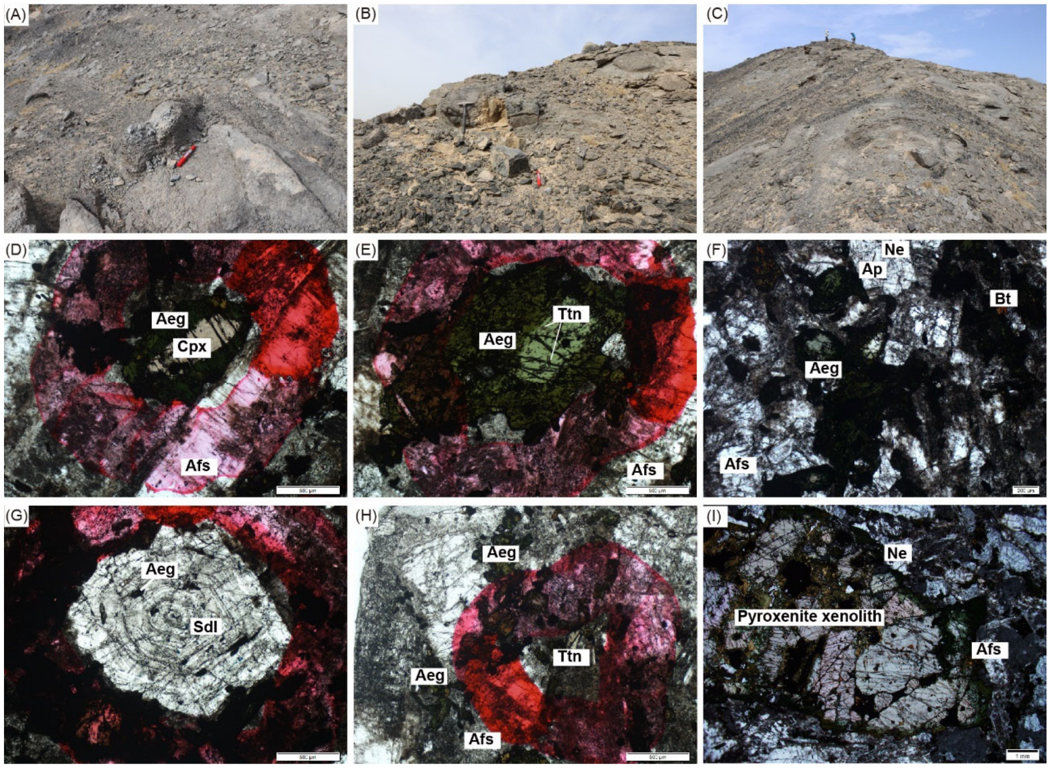

Figure S1. Field photographs (A, B and C) and photomicrographs (D to I) of the nepheline syenite (plane-polarized light). (D) Clinopyroxene showing the core is diopside; (E) The titanite grains enclosed in the clinopyroxene; (F) The potassium feldspar, aegirine-augite, apatite and biotite in the nepheline syenite, and the apatite enclosed in the nepheline; (G) Aegirine-augite grains enclosed in the sodalite; (H) The titanite in the nepheline syenite; (I) The pyroxenite xenolith in the nepheline syenite.

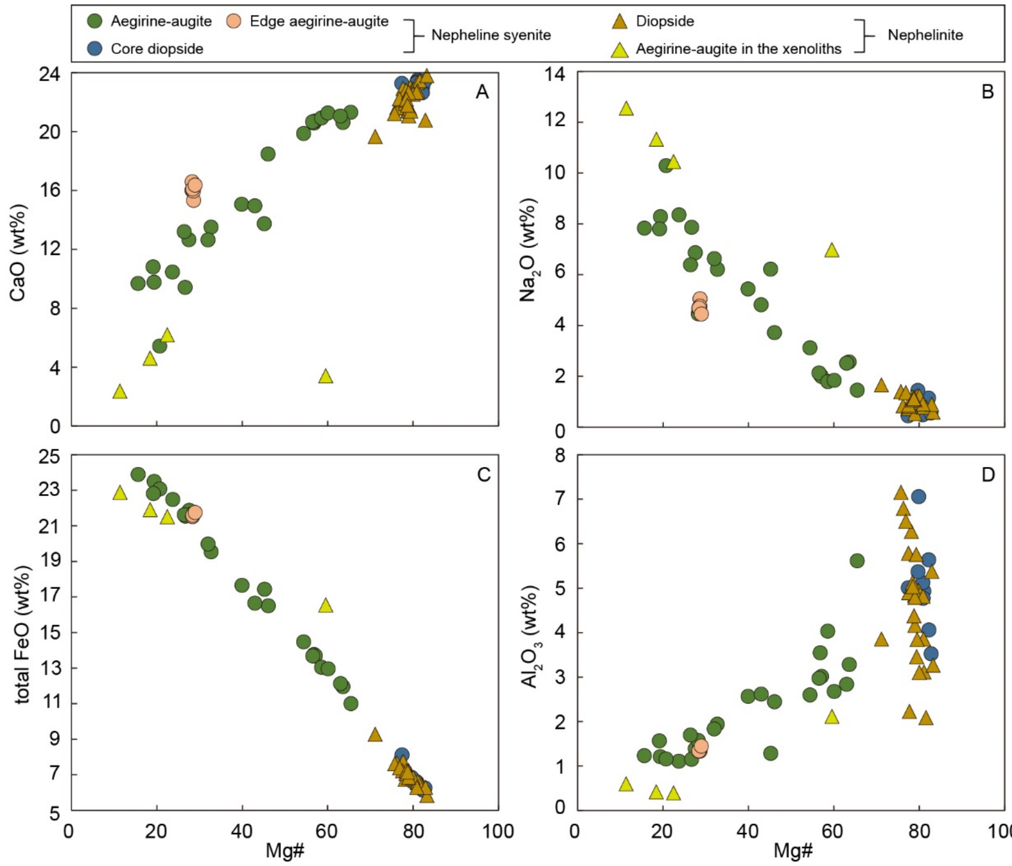

Figure S2. Harker diagram of major elements from clinopyroxene in nepheline syenite and nephelinite.

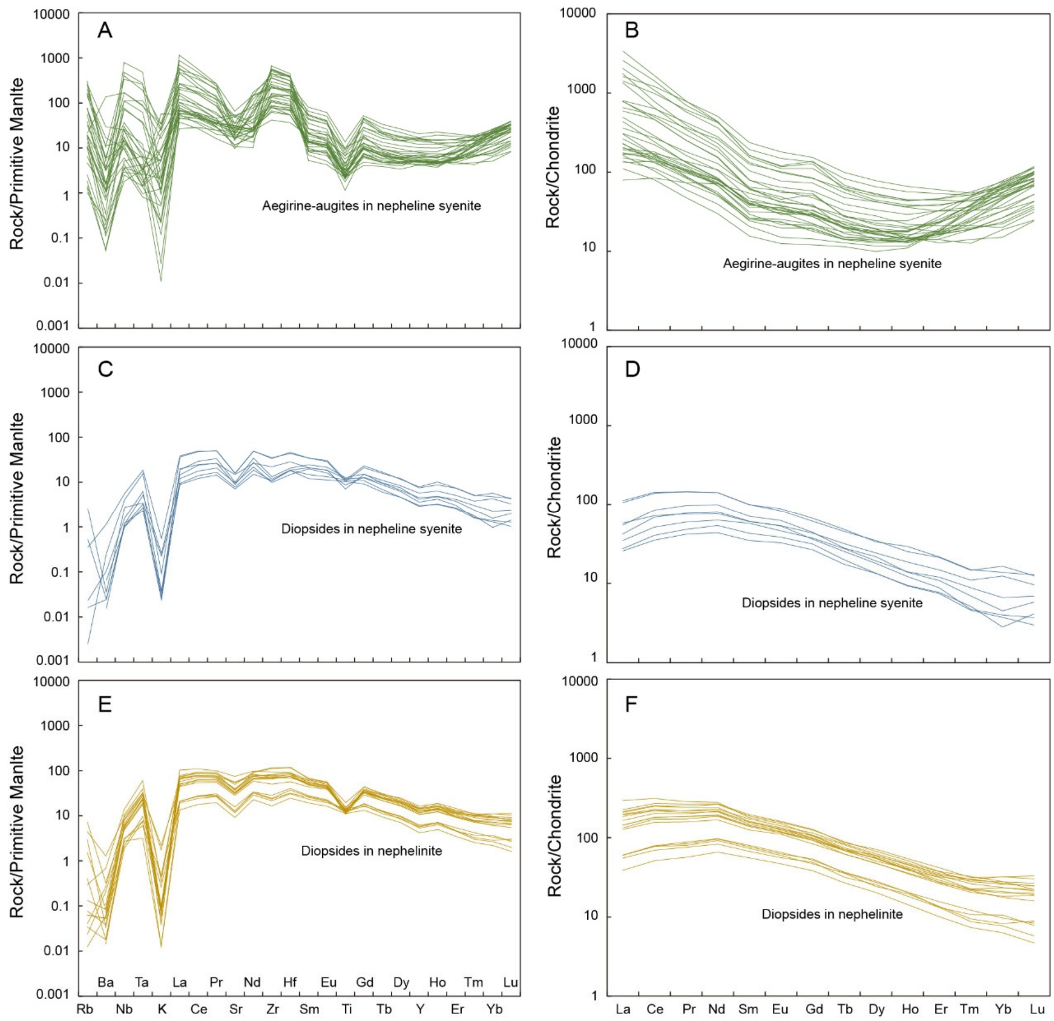

Figure S3. Primitive mantle-normalized trace element patterns (A, C and E) and chondrite-normalized rare earth element patterns (B, D and F) of the clinopyroxenes in Wajilitag nepheline syenite and nephelinite. Normalized values are after Sun and McDonough (1989).

REFERENCE CITED

Sun, S.S., McDonough, W.F., 1989, Chemical and isotopic systematics of oceanic basalts: implications for mantle composition and processes: Geological Society London Special Publications, v. 42, p. 313–345, https://doi.org/10.1144/GSL.SP.1989.042.01.19.

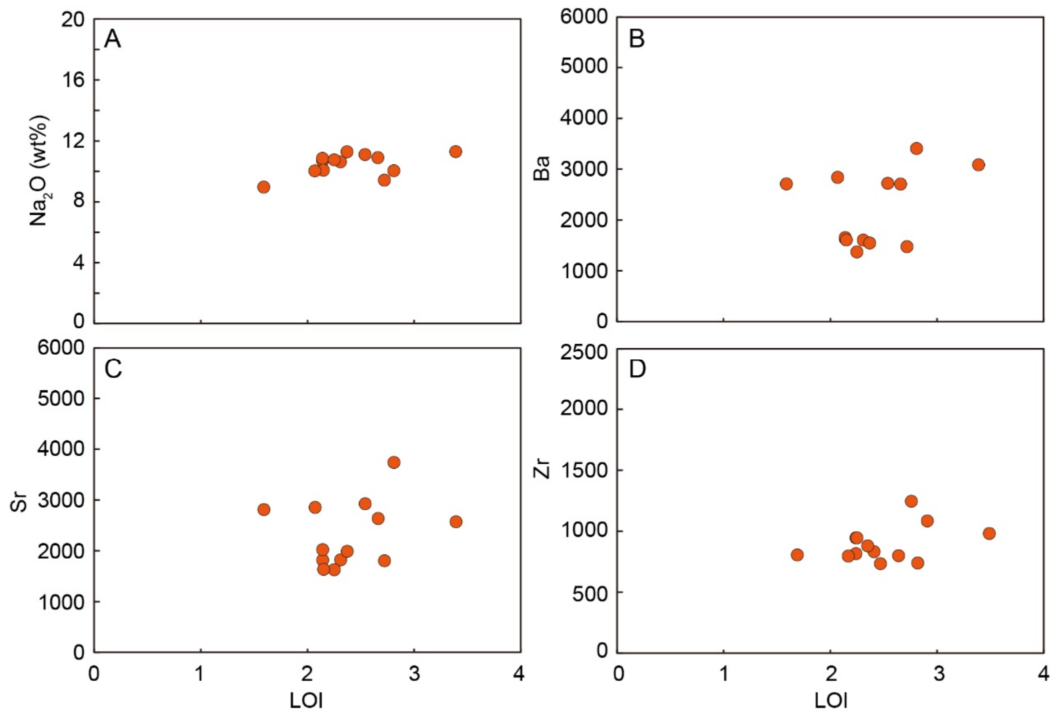

Figure S4. LOI versus Na₂O, Ba, Sr and Zr diagrams

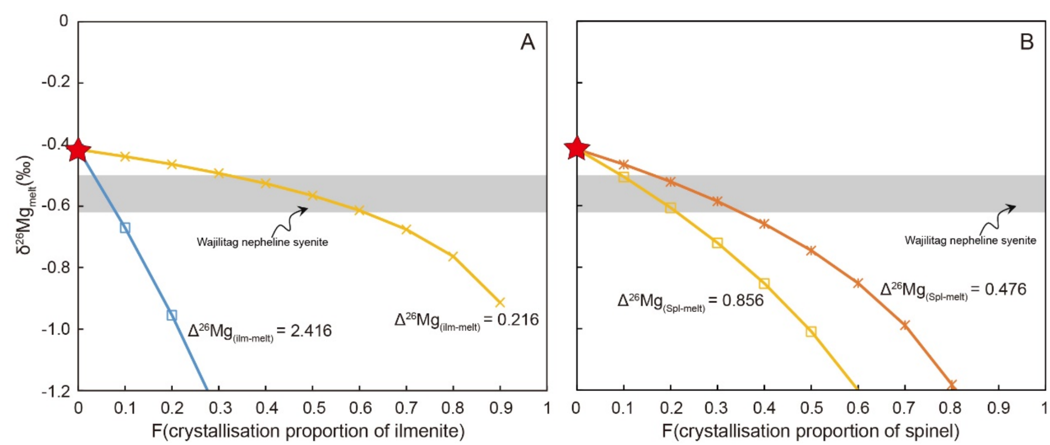

Figure S5. Rayleigh fractionation model showing the $\delta^{26}Mg$ evolution as fractional crystallization of ilmenite (A) and spinel (B). Modelling starts from the Wajilitag nephelinite (red star), where $\delta^{26}Mg$ = -0.416‰ (the average $\delta^{26}Mg$ value of nephelinites, n=10, Cheng et al., 2015). The gray bar represents the range of $\delta^{26}Mg$ values of the Wajilitag nepheline syenite of NW China (this study).

REFERENCE CITED

Cheng, Z.G., Zhang, Z.C., Hou, T., Santosh, M., Zhang, D.Y., and, Ke S., 2015, Petrogenesis of nephelinites from the Tarim Large Igneous Province, NW China: Implications for mantle source characteristics and plume–lithosphere interaction: Lithos, v. 220–223, p. 164–178, https://doi.org/10.1016/j.lithos.2015.02.002.